Int. J. Solids Structures Vol. 16, pp. 825–845
Pergamon Press Ltd., 1980. Printed in Great Britain

EFFECT OF GRAIN BOUNDARY SLIDING ON ANELASTICITY OF POLYCRYSTALS

F. GHAHREMANI
Division of Applied Sciences, Harvard University Cambridge, MA 02138, U.S.A.

(*Received* 16 *April* 1979)

Abstract—By using the finite element method and a self-consistent theory, the effect of grain boundary sliding on anelasticity of polycrystalline materials is analyzed. In the finite element calculations grains are modeled by a two-dimensional array of regular hexagons in plane strain. A Newtonian viscous relation is assigned to the grain boundaries. The ratio of the relaxed to the unrelaxed shear modulus, $\bar{G}/G$ and the relaxation time associated with grain boundary relaxation are calculated as a function of Poisson's ratio and the complex viscoelastic modulus is computed as a function of frequency. It is shown heuristically that the two-dimensional plane strain results may reasonably approximate the corresponding three-dimensional solution. In the self-consistent calculations it is assumed that the grains are spherical. The relation of this theory with that of Zener[4] is established.

1. INTRODUCTION

When accommodated only by the elastic distortion of the grains themselves, viscous slip at grain boundaries leads to anelastic behavior of polycrystalline metals at high temperatures. The shearing stresses relax across the grain boundaries, but the relative motion of grains is hindered at the corners where three grains meet. This relaxation of the shearing stresses gives rise to a relaxed shear modulus $\bar{G}$ which is less than G, the unrelaxed shear modulus. When a specimen of polycrystalline material is subjected to cyclic loading, slip at the grain boundaries contributes to the dissipation of mechanical energy into heat energy. Under steady state sinusoidal motion of frequency ω, the stress and strain at a point in the material are in general out of phase. The behavior of the material is determined by the complex viscoelastic modulus. The ratio of the imaginary part of the complex modulus to its real part is a measure of internal dissipation. In this paper we use continuum models to estimate the ratio $\bar{G}/G$ and to calculate the complex viscoelastic moduli as a function of frequency. For a comprehensive review of the literature see [1–3]. We recall briefly the relevant existing theoretical results.

One of the earliest significant works on grain boundary sliding is that of Zener[4] who attempted to calculate analytically the ratio of the relaxed to the unrelaxed elastic moduli. He modeled the grains by elastic isotropic spheres and compared the elastic energy stored in an individual grain under uniform stress with one under conditions of zero shearing stress across the boundary, requiring the average of the stress tensor to be the same in each case. In this way he obtained

$$\frac{\bar{G}}{G}=\frac{2(7+5\nu)}{5(7-4\nu)} \tag{1}$$

where ν is the Poisson's ratio of the grain material. An objection to this model is that it represents the polycrystal as an aggregate of spherical grains. Topologically, spheres differ from grains in two important ways, as far as the sliding at the boundary is concerned. Firstly, spheres do not pack to fill the space and secondly they have no corners.

Since on the average the shape of the grains is very complicated, the construction of a three-dimensional theory for grain boundary sliding with non-spherical grains is extremely difficult. A possible approach is the self-consistent theory developed by O'Connell and Budiansky[5, 6]. They modeled the grain boundaries by randomly oriented flat cracks filled with viscous fluid. Their analysis can be used to calculate $\bar{G}/G$ and the complex viscoelastic moduli for various grain shapes.

Another approach is to model the grain structure by a two-dimensional array of regular hexagons in plane strain as shown in Fig. 1. In Sections 2–4 of this paper we consider this

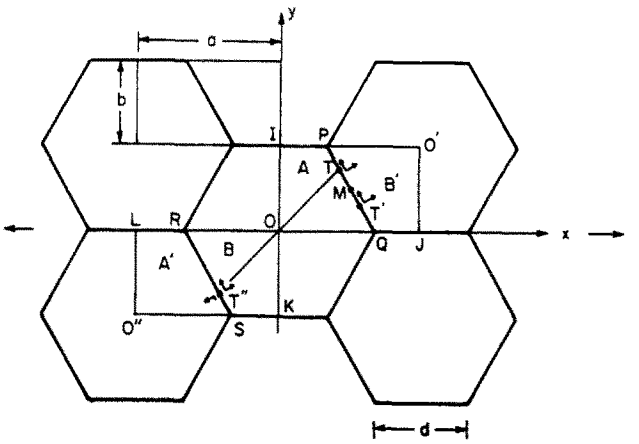

Fig. 1. Two-dimensional array of regular hexagons.

model. The material inside the grains is assumed to be linear and isotropically elastic. A Newtonian viscous relation is assigned to the grain boundaries. Thus, along the boundaries the shear stress σ_t is related to the jump in the tangential component of the velocity $[\dot{U}_t]$, by

$$\sigma_t = \frac{\eta}{w}[\dot{U}_t] \tag{2}$$

where η is the viscosity and w the thickness of the grain boundary. We use the finite element method to calculate $\bar{G}/G$ and the complex viscoelastic moduli. Crossman and Ashby considered the case when the material inside the grains is nonlinear. We have also performed calculations in the nonlinear range. The results can be found in [8] and will be published in a separate paper.

Finally in Section 5, we shall consider the implications of a different kind of self-consistent theory in which it is assumed that a grain behaves like a spherical inclusion in an infinite medium called the matrix. The inclusion has the unrelaxed elastic properties, and the matrix, the relaxed ones. Across the interface, the shearing stress vanishes and the normal component of the displacement vector is continuous. We shall establish the relation of this theory to that of Zener.

2. PRELIMINARY DISCUSSION

Consider the model polycrystal shown in Fig. 1 which is simply a two-dimensional array of regular hexagons in plane strain. The overall macroscopic stress is uniform tension in the x-direction. Because of the slip at the boundaries the local microscopic state of stress is non-uniform. The normal component of the displacement vector must be continuous across the grain boundaries, whereas its tangential component may suffer a jump. Also, no relative displacement of the grains is allowed to take place at the corners.

Let us denote by region A the trapezoid $OIPQ$ shown in Fig. 1. If the state of stress in region A is known, by symmetry it is also known everywhere in the entire array. Therefore, provided one is able to derive the boundary conditions for region A and solve the resulting boundary value problem, then the local stresses and strains (or strain rates) are everywhere known.

The boundary conditions for region A will now be derived. By symmetry every side of the rectangular region $OIO'J$ in Fig. 1 remains straight as a result of an overall stress in the x-direction. Furthermore, the shearing stress must vanish on every side. Let $U(x, y)$ and $V(x, y)$ denote the displacements in the x and y directions. Assume at the origin, point O, $U = V = O$ and at the point O', $U = u$ and $V = v$. Then for region A

$$\begin{cases} U = O & \tau_{xy} = O & \text{on } OI \\ V = O & \tau_{xy} = O & \text{on } OQ \\ V = v & \tau_{xy} = O & \text{on } IP. \end{cases} \tag{3}$$

This gives the complete boundary conditions on OI, OQ and IP.

To derive the boundary conditions on PQ, which are more complicated, we first need to find a formula relating the displacement vector in the region B' (the trapezoid $O'JQP$ in Fig. 1) to that in region A. This formula is derived by using symmetry arguments. For a point (x, y) in B', $(a-x, b-y)$ is in A, where a and b are the length and the width of rectangle $OIO'J$; then one has

$$\mathbf{U}(x, y) = -\mathbf{U}(a-x, b-y) + \mathbf{u} \qquad (x, y) \text{ in } B' \tag{4}$$

where $\mathbf{U} = U\mathbf{i} + V\mathbf{j}$ and $\mathbf{u} = u\mathbf{i} + v\mathbf{j}$.

Now consider the boundary condition that the normal component of the displacement vector must be continuous across PQ. At a point $T:(x, y)$ on PQ, the normal displacement in region A is $U_n^{(A)}(x, y) = U_n(x, y)$. At the same point but considered in B' by (4)

$$U_n^{(B')}(x, y) = -U_n(a-x, b-y) + u_n$$

where $u_n = \sqrt{3}u/2 + v/2$ is the normal component of $\mathbf{u}$. Therefore, setting $U_n^{(A)}(x, y) = U_n^{(B')}(x, y)$ one gets

$$U_n(x, y) + U_n(a-x, b-y) = u_n \qquad (x, y) \text{ on } PQ. \tag{5}$$

This equation expresses the requirement of continuity of normal displacement across the boundary. It is a relation between the normal component of the displacement vector at points $T:(x, y)$ and $T'(a-x, b-y)$ on the boundary. These two points are equidistant from M, where $M:(a/2, b/2)$ is the midpoint of the segment PQ in Fig. 1. Similarly, we derive the following two useful formulas which are not boundary conditions but will be used in the future. The condition that no relative displacement is allowed at the triple points P and Q gives

$$\mathbf{U}(x_P, b) + \mathbf{U}(x_Q, 0) = \mathbf{u}. \tag{6}$$

The jump in the tangential component of the displacement vector as one crosses the boundary PQ from region A to B' is

$$U_t^{(B')}(x, y) - U_t^{(A)}(x, y) = u_t - U_t(a-x, b-y) - U_t(x, y) \tag{7}$$

where $u_t = -u/2 + \sqrt{3}v/2$ is the tangential component of $\mathbf{u}$.

On each side of the region A, a normal and a tangential boundary condition must be specified. For example, on OI by (3) $U = 0$ and $\tau_{xy} = 0$ are the normal and the tangential boundary conditions. The tangential boundary condition on PQ will be derived later. Consider now the normal boundary condition on this side. Equation (5) is a condition for normal displacement. But since this is only a relationship between normal displacements at two different points on the boundary, it is not by itself sufficient. Another boundary condition in the normal direction must be given.

Referring to Fig. 1, from symmetry it can be shown that at points equidistant from M on the boundary the traction vector must be equal, i.e.

$$\begin{cases} \sigma_n(x, y) = \sigma_n(a-x, b-y) & \text{(8a)} \\ \sigma_t(x, y) = \sigma_t(a-x, b-y) & \text{(8b)} \end{cases} \qquad \text{on } PQ$$

where σ_n and σ_t are the normal and the tangential components of the traction vector on PQ. Equation (8a) along with (5) constitutes the complete boundary condition in the normal direction. In addition, the tangential boundary conditions on PQ must be consistent with (8b).

3. RELAXED ELASTIC MODULI

In this section the ratio of the relaxed to the unrelaxed shear modulus, $\bar{G}/G$, will be calculated. The shearing stresses across the grain boundaries are completely relaxed. The

tangential boundary condition on PQ of Fig. 1 is $\sigma_t = 0$. This, together with (3), (5), and (8a) gives the complete boundary condition for region A except for one more small detail. These boundary conditions must be consistent with an overall applied stress system $\bar{\sigma}_x = \bar{\sigma}$ and $\bar{\sigma}_y = \bar{\tau}_{xy} = 0$. Since $\tau_{xy} = 0$ on every side of the representative rectangle $OIO'J$ in Fig. 1, the condition $\bar{\tau}_{xy} = 0$ is obviously satisfied. Therefore one must have

$$\begin{cases} \bar{\sigma}_x = \dfrac{1}{b}\displaystyle\int_{OI} \sigma_x \, dy = \bar{\sigma} & (9) \\ \bar{\sigma}_y = \dfrac{1}{a}\displaystyle\int_{IP} \sigma_y \, dx + \dfrac{1}{a}\int_{OQ} \sigma_y \, dx = 0. & (10) \end{cases}$$

Evidently, (9) and (10) should be regarded as equations for the quantities u and v which appear in the boundary conditions (3) and (5). In the following calculations it is more convenient to specify v rather than $\bar{\sigma}_x$; then, (9) will be used to determine $\bar{\sigma}_x$, and (10) will be regarded as a constraint that can be used to find u. Figure 2(a) shows the complete boundary conditions for region A.

The plane-strain stress-strain relations for the material inside the grains are derived from Hooke's law for an isotropic elastic solid, i.e. the equations

$$\begin{cases} \epsilon_x = \dfrac{1}{E}(\sigma_x - \nu\sigma_y) - \dfrac{\nu}{E}\sigma_z \\ \epsilon_y = \dfrac{1}{E}(\sigma_y - \nu\sigma_x) - \dfrac{\nu}{E}\sigma_z \\ \gamma_{xy} = \dfrac{1}{G}\tau_{xy}; \quad G = \dfrac{E}{2(1+\nu)} \end{cases} \tag{11}$$

and

$$\epsilon_z = \frac{1}{E}\sigma_z - \frac{\nu}{E}(\sigma_x + \sigma_y). \tag{12}$$

It is obvious that the plane strain configuration of the hexagonal polycrystal, shown in Fig. 1, has a sixth order axis of symmetry along the z-axis. It can be shown that a linearly elastic solid with an axis of symmetry of the sixth order is transversely isotropic with respect to that axis [9]. Therefore, the overall response of our idealized polycrystal is necessarily transversely isotro-

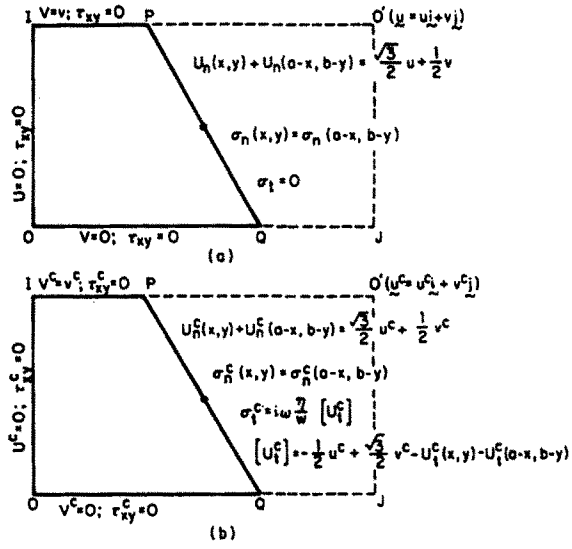

Fig. 2. Boundary conditions, (a) completely relaxed, (b) complex.

pic. In other words, the direction of an overall applied uniaxial stress is immaterial in this linear analysis. The response of the polycrystal in the xy-plane is (from Hooke's law for a transversely isotropic elastic solid)

$$\begin{cases} \bar{\epsilon}_x = \dfrac{1}{\bar{E}}(\bar{\sigma}_x - \bar{\nu}\bar{\sigma}_y) - \dfrac{\nu}{E}\bar{\sigma}_z \\ \bar{\epsilon}_y = \dfrac{1}{\bar{E}}(\bar{\sigma}_y - \bar{\nu}\bar{\sigma}_x) - \dfrac{\nu}{E}\bar{\sigma}_z \\ \bar{\gamma}_{xy} = \dfrac{1}{\bar{G}}\bar{\tau}_{xy}; \quad \bar{G} = \dfrac{\bar{E}}{2(1+\bar{\nu})} \end{cases} \tag{13}$$

where $\bar{E}$, $\bar{\nu}$, and $\bar{G}$ are the relaxed elastic constants. In the z-direction no relaxation occurs and (12) still holds.

In plane strain, with $\epsilon_z = 0$, (11) and (12) give, within the grains

$$\begin{cases} \epsilon_z = \dfrac{1}{E}(\sigma_x - \nu\sigma_y) - \dfrac{\nu^2}{E}(\sigma_x + \sigma_y) \\ \epsilon_y = \dfrac{1}{E}(\sigma_y - \nu\sigma_x) - \dfrac{\nu^2}{E}(\sigma_x + \sigma_y) \\ \gamma_{xy} = \dfrac{1}{G}\tau_{xy}; \quad G = \dfrac{E}{2(1+\nu)}. \end{cases} \tag{14}$$

Similarly, from (13) and (12) the overall plane strain equations are

$$\begin{cases} \bar{\epsilon}_x = \dfrac{1}{\bar{E}}(\bar{\sigma}_x - \bar{\nu}\bar{\sigma}_y) - \dfrac{\nu^2}{E}(\bar{\sigma}_x + \bar{\sigma}_y) \\ \bar{\epsilon}_y = \dfrac{1}{\bar{E}}(\bar{\sigma}_y - \bar{\nu}\bar{\sigma}_x) - \dfrac{\nu^2}{E}(\bar{\sigma}_x + \bar{\sigma}_y) \\ \bar{\gamma}_{xy} = \dfrac{1}{\bar{G}}\bar{\tau}_{xy}; \quad \bar{G} = \dfrac{\bar{E}}{2(1+\bar{\nu})}. \end{cases} \tag{15}$$

Equations (14) and (15) indicate that it is not correct to represent the overall stress–strain relations by simply putting a bar over every coefficient in (14); since the model is two-dimensional, the coefficient of $\sigma_x + \sigma_y$ (i.e. ν^2/E) does not relax.

If the state of stress in the xy-plane is isotropic, i.e., $\sigma_x = \sigma_y$ and $\tau_{xy} = 0$, then the shearing stress on every plane vanishes and no relaxation occurs, so that $\sigma_x = \bar{\sigma}_x = \bar{\sigma}_y = \sigma_y$, $\epsilon_x = \bar{\epsilon}_x = \bar{\epsilon}_y = \epsilon_y$ and $\gamma_{xy} = \bar{\gamma}_{xy} = \tau_{xy} = \bar{\tau}_{xy} = 0$. From (14) and (15) it follows that

$$\frac{1-\bar{\nu}}{\bar{E}} = \frac{1-\nu}{E}. \tag{16}$$

This equation expresses the fact that the two-dimensional elastic bulk modulus is not affected by grain boundary relaxation.

In terms of the quantities involved in the calculations, the overall strains are given by

$$\begin{cases} \bar{\epsilon}_x = \dfrac{u}{a} \\ \bar{\epsilon}_y = \dfrac{v}{b}. \end{cases} \tag{17}$$

From (10) $\bar{\sigma}_y = 0$, and $\bar{\sigma}_x$ is computed using (9). The first equation in (15) gives $\bar{E}$ as determined

by the computed ratio $\bar{\epsilon}_x/\bar{\sigma}_x$, i.e.

$$\bar{E} = \frac{1}{\frac{\bar{\epsilon}_x}{\bar{\sigma}_x} + \frac{\nu^2}{E}}. \tag{18}$$

And from the second equation in (15)

$$\bar{\nu} = -\bar{E}\left(\frac{\bar{\epsilon}_y}{\bar{\sigma}_x} + \frac{\nu^2}{E}\right). \tag{19}$$

Also the relaxed shear modulus $\bar{G}$ may be found from

$$\bar{G} = \frac{\bar{\sigma}_x}{2(\bar{\epsilon}_x - \bar{\epsilon}_y)} \quad \text{or} \quad \bar{G} = \frac{\bar{E}}{2(1+\bar{\nu})}. \tag{20}$$

In addition, these calculated quantities must satisfy eqn (16) as a check.†

The finite element solution

A finite element approach for plane strain analysis can be used to solve approximately the elastostatic boundary value problem posed for region A. The details are given in part A.1 of the Appendix. The main difficulty is caused by the boundary conditions shown in Fig. 2(a). Since these boundary conditions are rather uncommon, a general-purpose finite element program capable of handling them is not available. In the next section we encounter boundary conditions even more complicated than the ones seen here. In the appendix we describe a method that can be used to implement all of these boundary conditions effectively. Application of this method requires some extra programming effort but not much additional computer time.

Results and discussion

The finite element grid used is shown in Fig. 3(a). This grid has 756 constant strain triangular elements per grain. (Notice that each quadrilateral in Fig. 3(a) is composed of four triangles.) By using the much finer grid shown in Fig. 3(b), which has 1452 elements per grain, it was found that the results for $\bar{G}/G$ remain essentially unchanged. In Fig. 4, the curve labeled (1) shows $\bar{G}/G$ as a function of ν, as found with the grid of Fig. 3(a). Point (X) was obtained in[8] by means of a finite element program written for strictly incompressible materials. It can be seen that this point is in complete agreement with curve (1) when ν approaches $\frac{1}{2}$. Point (*) is the result of the finite element calculations by Crossman and Ashby[7].

The curve labeled (2) was obtained by Raj and Ashby[10]. They used an approximate method based on Fourier series. As will be shown at the end of the next section, the Budiansky–O'Connell self-consistent analysis[5, 6] applied to plane-strain hexagonal grains gives a result which is almost identical to that of Raj and Ashby.

Having carried out these finite element calculations for two-dimensional grains, one is left with the task of interpreting the results for three-dimensional grains. Some insight into this may be gained by performing Zener's calculation in two dimensions for a circular grain in plane strain rather than for a sphere and comparing the result with the Zener eqn (11). This calculation is carried out in A.3 of the Appendix. The result is plotted as the curve (3) in Fig. 4. The Zener equation for spherical grains is curve (4). Over the usual range of Poisson's ratio of 0.3–0.4, the plane strain value for $\bar{G}/G$ is slightly larger than Zener's three dimensional result. This suggests, at least heuristically, that a two-dimensional plane strain solution may indeed reasonably approximate the corresponding three-dimensional solution as far as the ratio $\bar{G}/G$ is concerned.

†In the above procedure an arbitrary value is assigned to v, but u is left free and solved for so that $\bar{\sigma}_y = 0$. In effect, $\bar{\epsilon}_y$ and $\bar{\sigma}_y$ are assigned and $\bar{\sigma}_x$ and $\bar{\epsilon}_x$ are computed. If an arbitrary value is assigned to u as well as to v, from (10) it will be found that $\bar{\sigma}_y \neq 0$. Then $\bar{\epsilon}_x$ and $\bar{\epsilon}_y$ are assigned and $\bar{\sigma}_x$ and $\bar{\sigma}_y$, computed; the first two equations in (15) solved simultaneously in terms of the assigned ($E, \nu, \bar{\epsilon}_x, \bar{\epsilon}_y$) and the computed ($\bar{\sigma}_x, \bar{\sigma}_y$) quantities give $\bar{E}$ and $\bar{\nu}$. Although we employed the former procedure, the latter is simpler to implement since in that case the constraint (10) ($\bar{\sigma}_y = 0$), need not be imposed.

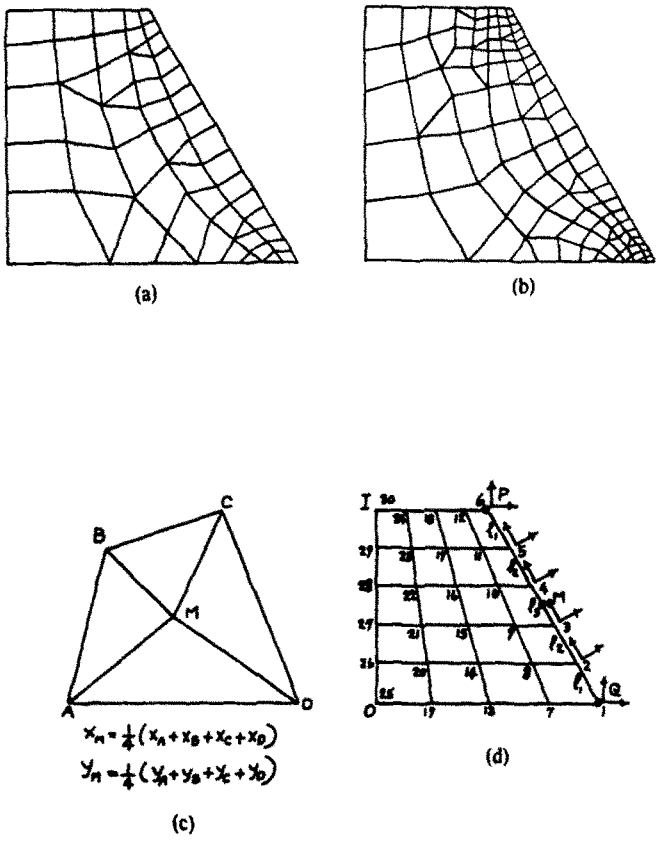

Fig. 3. (a), (b) Finite element grids, (c) quadrilateral element, (d) a typical finite element grid.

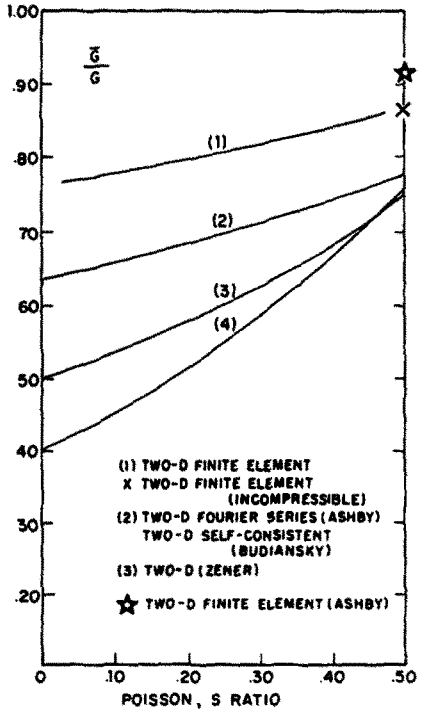

Fig. 4. The ratio $\bar{G}/G$ vs ν.

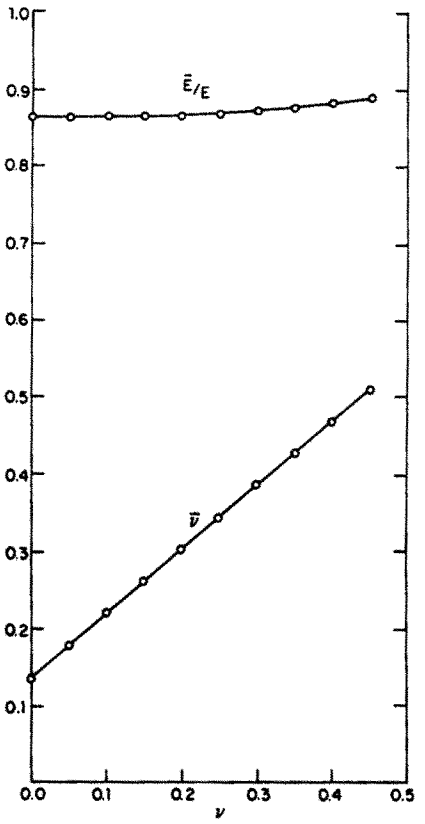

Fig. 5. Relaxed Poisson's ratio and $\bar{E}/E$ vs ν.

Figure 5 shows $\bar{E}/E$ and $\bar{\nu}$ as a function of ν as computed by our finite element program. These results satisfy eqn (16) as a check. It can be seen that $\bar{\nu}$ appears to be very nearly a linear function of ν. Assuming $\bar{\nu}$ to be linear and using (16), one finds

$$\begin{cases} \bar{\nu} \approx 0.83\nu + 0.14 \\ \dfrac{\bar{E}}{E} \approx \dfrac{0.83\nu - 0.86}{\nu - 1}. \end{cases} \tag{21}$$

These equations describe the numerical results quite satisfactorily.

4. COMPLEX VISCOELASTIC MODULI

When the overall applied stress is a sinusoidal function of time with frequency ω, all quantities (displacements, stresses, etc.) are also sinusoidal functions of time with frequency ω. If no internal relaxation of any kind takes place, the strain must be in phase with the stress, but as a result of relaxation the strain in general lags behind the stress. In our model there is only one mechanism of internal relaxation operating in the material, i.e. the relaxation of shearing stresses at the grain boundaries. The local stresses (i.e. the stresses inside the hexagonal grains) remain in phase with the local strains.

It is convenient to introduce complex notation. Let a quantity, e.g. σ, be of the form $\sigma = \sigma_1 \cos \omega t + \sigma_2 \sin \omega t$. We shall write this as

$$\begin{cases} \sigma = \sigma^R \cos \omega t - \sigma^I \sin \omega t = \mathrm{Re}\,(\sigma^*), \quad \text{where} \\ \sigma^* = \sigma^C e^{i\omega t} = (\sigma^R + i\sigma^I)(\cos \omega t + i \sin \omega t), \quad \text{and} \\ \sigma^C = \sigma^R + i\sigma^I. \end{cases} \tag{22}$$

The superscript C means complex and σ^R and σ^I are the real and the imaginary parts of σ^C.

Grain boundary relaxation is significant in a frequency range for which the period is comparable to the time of relaxation of shearing stresses. Since this relaxation time is relatively large, the corresponding period is sufficiently large so that the inertia forces can be neglected compared to the elastic forces in the grains and the viscous forces at the grain boundaries. Then it can easily be seen that the complex displacements $U^C(x, y)$ and $V^C(x, y)$ satisfy the ordinary plane strain equations of elastostatics. It only remains to derive the boundary conditions for these displacements.

For the trapezoidal region $OIPQ$ shown in Fig. 1, it can easily be seen that the boundary conditions on OI, OQ and IP are obtained from (3) by adding the superscript C to every variable. Similarly on PQ, eqn (6) and the normal boundary conditions (5) and (8a) hold for the corresponding complex quantities.

The tangential boundary condition on PQ is obtained by substituting $\sigma_t^* = \sigma_t^C e^{i\omega t}$ and $U_t^* = U_t^C e^{i\omega t}$ ($\dot{U}_t^* = i\omega U_t^C e^{i\omega t}$) in (2) and canceling $e^{i\omega t}$; this gives

$$\sigma_t^C = i\omega \frac{\eta}{w} [U_t^C] \tag{23}$$

where from (7) the jump in the tangential component of the complex displacement vector across PQ is

$$[U_t^C] = u_t^C - U_t^C(x, y) - U_t^C(a - x, b - y) \tag{24}$$

and $u_t^C = -u^C/2 + \sqrt{3}v^C/2$ is the tangential component of u^C. Equations (23) and (24) determine the tangential boundary condition on PQ.

In addition to the above boundary conditions we have the complex version of (9) and (10). As in Section 3 an arbitrary real value will be assigned to v^C and (10) will be used as an equation for the determination of u^C. The complete boundary conditions in the complex form are shown in Fig. 2(b). The complex boundary value problem for region A is now completely defined.

The overall strains $\bar{\epsilon}_x^C$, $\bar{\epsilon}_y^C$ are calculated by using the complex form of (17). By (10) $\bar{\sigma}_y^C = 0$ and $\bar{\sigma}_x^C$ is calculated using (9). The maximum overall shearing stress is $\bar{\tau}^C = (\bar{\sigma}_y^C - \bar{\sigma}_y^C)/2 = \bar{\sigma}^C/2$. The maximum overall shearing strain is $\bar{\gamma}^C = \bar{\epsilon}_x^C - \bar{\epsilon}_y^C$. Then,

$$G^C = \frac{\bar{\tau}^C}{\bar{\gamma}^C} \tag{25}$$

is the complex shear modulus of the polycrystal.

At sufficiently low frequencies, $\omega \approx 0$, by (23) $\tau^C \approx 0$ and the boundary conditions on PQ are almost the same as in Section 3. The material is then essentially completely relaxed. Its transversely isotropic constitutive equation is (15). On the other hand, at sufficiently high frequencies since τ^C is finite, $\tau^C/\omega \approx 0$ or by (23) $[U_t^C] \approx 0$. That is, the jump in the tangential component of the displacement vector across the boundary is nearly zero. The material is now essentially completely unrelaxed. Its isotropic constitutive equation is (14). Therefore, at the two extremes, for sufficiently large and sufficiently small ω, the material is transversely isotropic. At intermediate frequencies, using the concept of an operational tensor, it can be shown that the polycrystal is still transversely isotropic[11].

The transverse isotropy of the polycrystal implies that the overall and local responses to an isotropic stress system ($\bar{\sigma}_x = \bar{\sigma}_y$ and $\bar{\tau}_{xy} = 0$) are the same. This fact can be used to derive the following relation between the computed quantities $\bar{\epsilon}_x^C$ and $\bar{\sigma}_x^C$:

$$\bar{\epsilon}_x^C + \bar{\epsilon}_y^C = \frac{(1+\nu)(1-\nu)}{E} \bar{\sigma}_x^C. \tag{26}$$

This equation, which is the counterpart of (16), is a check on calculations.

Finite element discretization

The finite element technique in this section, although more complicated, is very similar to

that of Section 3. The grid shown in Fig. 3(a) is used again. Because of the boundary conditions the computations must be carried out in complex mode. The complete details are given in A.2 of the Appendix.

Numerical results

We first briefly recall some concepts. The standard linear solid obeys an equation of the form[1]

$$\tau + \tau_\epsilon \dot{\tau} = \bar{G}(\gamma + \tau_\sigma \dot{\gamma}) \tag{27}$$

where the material constants τ_ϵ and τ_σ are relaxation times at constant strain and stress respectively, $\bar{G}$ is the relaxed shear modulus, and a dot denotes differentiation with respect to time. Substituting $\tau^* = \tau^C e^{i\omega t}$ and $\gamma^* = \gamma^C e^{i\omega t}$, canceling $e^{i\omega t}$ and using the definition $\tau^C = G^C \gamma^C (G^C = G^R + iG^I)$ one obtains the Debye equations

$$\begin{cases} G^R = G - \dfrac{\delta G}{1 + \omega^2 \tau_\epsilon^2} \\ G^I = \delta G \dfrac{\omega \tau_\epsilon}{1 + \omega^2 \tau_\epsilon^2} \end{cases} \tag{28}$$

where G is the unrelaxed shear modulus,

$$\frac{\bar{G}}{G} = \frac{\tau_\epsilon}{\tau_\sigma} \tag{29}$$

and $\delta G = G - \bar{G}$.

With the help of these formulas the result of the computations will be explained. Using (25) one can calculate the complex shear modulus as a function of $\ln(\omega)$. Figure 6(a) shows its imaginary part for $\nu = 0.35$. The points computed by the finite element program are designated by the circles. The frequency ω_c at which G^I is a maximum can be determined numerically. For $\nu = 0.35$ it was found that $\omega_c/(Ew/\eta d) \approx 1.1047$, where $\omega_c/(Ew/\eta d)$ is nondimensional and d is the length of a side of the hexagons.

On the other hand, for the standard linear solid, from (28) G^I can be written as

$$\frac{G^I}{G} = \frac{\delta G}{2G} \operatorname{sech}[\ln(\omega \tau_\epsilon)]. \tag{30}$$

This has a maximum when $\omega \tau_\epsilon = 1$; therefore

$$\tau_\epsilon = \frac{1}{\omega_c}. \tag{31}$$

From Section 3 for $\nu = 0.35$, $\delta G/2G = 0.08478$. Equation (30) is plotted as the dashed curve in Fig. 6(a). The close agreement between this curve and the computed points clearly indicates that the model behaves like the standard linear solid. The three parameters G, $\bar{G}$, and τ_ϵ completely define the standard linear solid. Since $\bar{G}/G$ was already calculated in Section 3, calculation of τ_ϵ completes the characterization of the material. Figure 6(b) shows the real part of the complex shear modulus, G^R, for the same value of ν as in Fig. 6(a). A smooth solid line is drawn through the computed points.

Dimensional analysis shows that in addition to $\bar{G}/G$ there is essentially just one more nondimensional quantity which is a function of ν and may be chosen as

$$\alpha = \frac{\eta D}{\tau_\sigma G w} = h(\nu) \tag{32}$$

where D, the grain diameter, will be taken as the diameter of a circle whose area is the same as

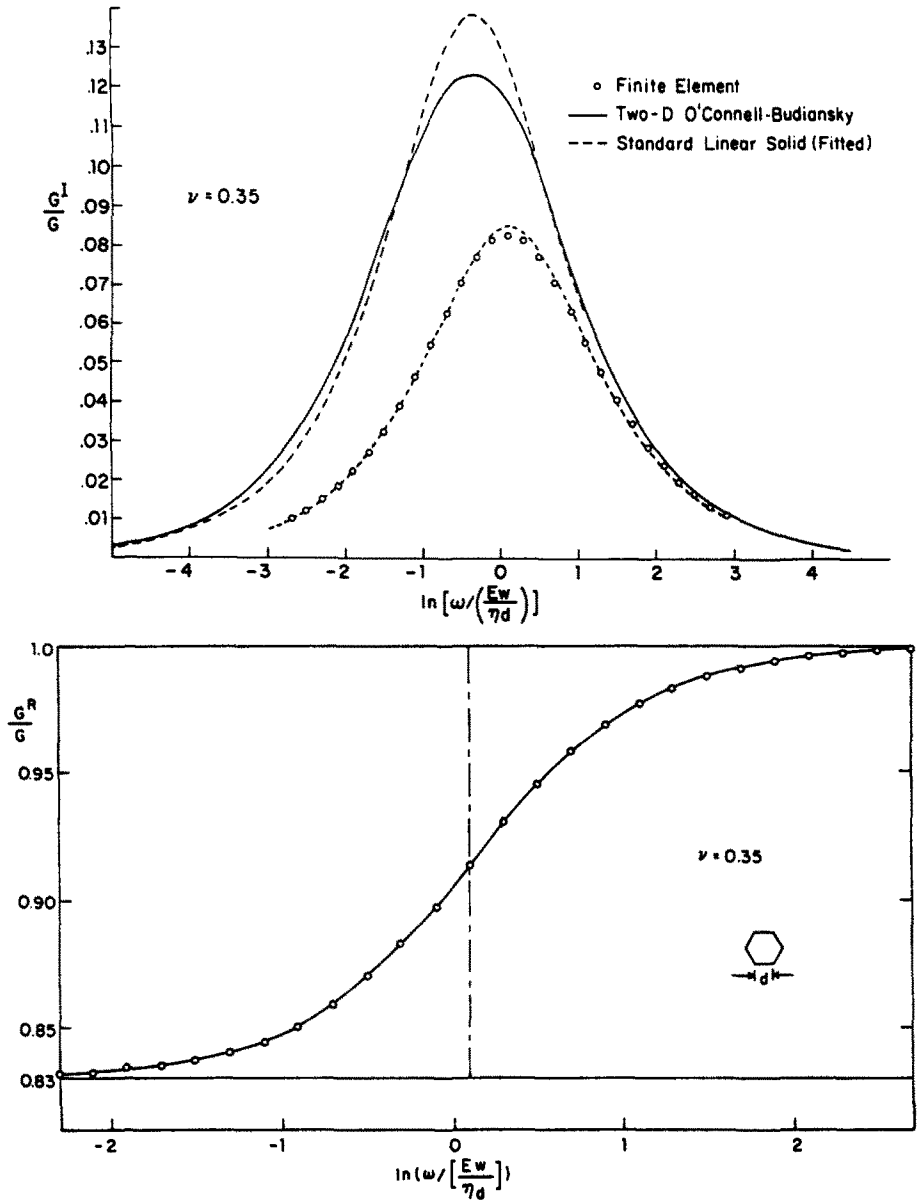

Fig. 6. Complex modulus, (a) G^I/G vs $\ln\left[\omega/\left(\frac{Ew}{\eta d}\right)\right]$, (b) G^R/G vs $\ln\left[\omega/\left(\frac{Ew}{\eta d}\right)\right]$.

that of the hexagons, or

$$D = 2d\sqrt{\left(\frac{3\sqrt{3}}{2\pi}\right)} \quad (d = \tfrac{2}{3}a) \tag{33}$$

The function $h(\nu) = \alpha$ as computed by the finite element program is plotted in Fig. 7(a). In (32) τ_ϵ and τ_σ were calculated using (31) and (29). The number α has also been calculated by other authors. By a crude estimation $K\hat{e}$[12] and Nowic and Berry[13] give $\alpha = 1$. A somewhat more sophisticated analysis by Smith[14], quoted in[2], resulted in $\alpha = b$.

Figure 7(b) shows the variation of τ_σ and τ_ϵ with ν. It can be seen that these quantities are rather weak functions of ν.

Comparison with the O'Connell–Budiansky theory

The O'Connell–Budiansky self-consistent calculations[5] will now be carried out in plane strain for hexagonal grains, and the results will be compared with ours. Consider a body permeated by many randomly oriented straight cracks filled with a fluid of viscosity η (the grain boundary viscosity). It is assumed that no fluid can flow out of any crack (saturated isolated

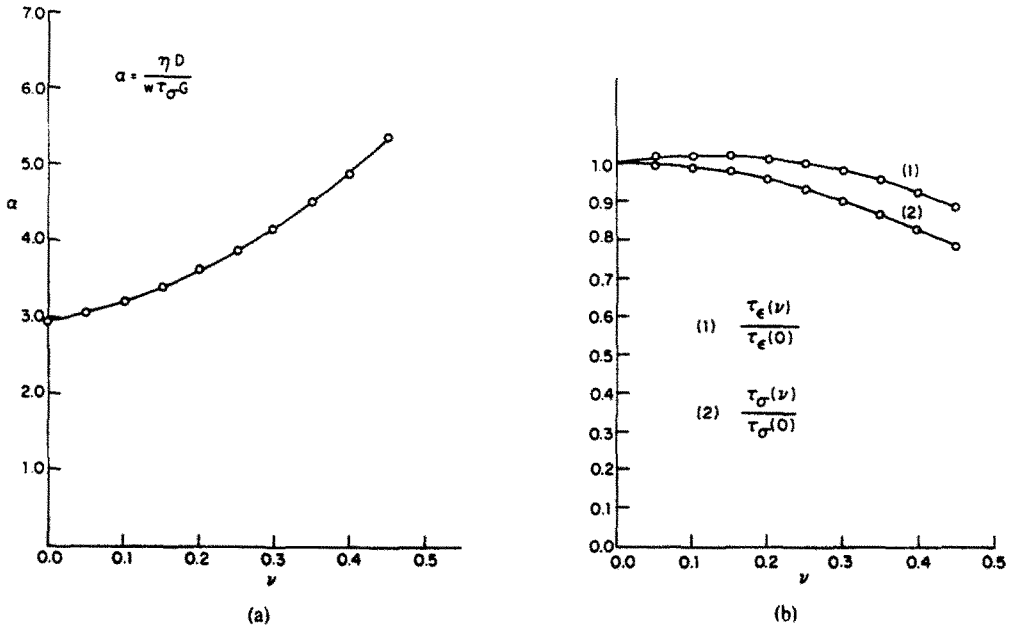

Fig. 7. (a) The number α vs ν, (b) variation of relaxation times with ν.

case [5]). The cracks are thin ellipses with major axis d (the length of the side of a hexagon) and minor axis h. The average width of an ellipse is the width of the grain boundary w, $\pi hd/4 = wd$ or $h = 4w/\pi$. As in [5], first assuming the cracks are thin inclusions which contain material with shear modulus $\bar{G}$, we find the effective elastic properties; then $\bar{G}$ will be replaced by $i\omega\eta$ to obtain the complex viscoelastic moduli.

Let the overall state of stress be uniform tension in the y-direction, $\bar{\sigma}_y = \sigma$. Then, remembering that the effective stress-strain equations are transversely isotropic and are similar to (15), one can write the energy balance equation as (see [6])

$$-\frac{A\sigma^2}{2}\left(\frac{1}{E_e}-\frac{\nu^2}{E}\right) = -\frac{A\sigma^2}{2}\left(\frac{1}{E}-\frac{\nu^2}{E}\right)+\Delta\phi \tag{34}$$

where A is the area of the body, E_e is the effective Young's modulus and $\Delta\phi$ is the potential energy change as a result of the introduction of the random set of inclusions in the body. The quantity $\Delta\phi$ will be estimated by calculating the energy loss produced by a single isolated inclusion in an infinite medium having the effective elastic properties. This loss in energy is [6]

$$\mathscr{E} = \frac{\pi d^2}{4}(\tau^2-\bar{\tau}^2)\left(\frac{1}{E_e}-\frac{\nu^2}{E}\right)-\frac{\bar{\tau}^2}{2\bar{G}}A_I \tag{35}$$

where $A_I = \pi dw/4$ is the area of the inclusion, $\tau = \sigma \sin\theta\cos\theta$ is the resolved shear stress on the surface of the inclusion whose major axis makes an angle θ with the x-axis, and $\bar{\tau}$ is the shearing stress in the inclusion. This can be calculated from

$$\frac{\bar{\tau}}{\bar{G}}A_I = \int_{S_I}(U_X n_Y + U_Y n_X)\,\mathrm{d}S_I$$

where S_I is the surface of the inclusion, $\mathbf{n}$ its unit outward normal and XY-axes coincide with the principal axes of the inclusion. Whence

$$\bar{\tau} = \frac{\tau}{1+\dfrac{h}{2\bar{G}d}\cdot\dfrac{1}{\dfrac{1}{E_e}-\dfrac{\nu^2}{E}}} \qquad \left(h=\frac{4}{\pi}w\right) \tag{36}$$

Averaging (35) over all orientations, substituting $G = i\omega\eta$ into (34), and replacing E_c by E^C, one gets

$$\frac{E^C}{E} = 1 - \left(\frac{\pi}{16}\right)\left(1 - \nu^2\frac{E^C}{E}\right)S(\omega)Nd^2 \tag{37}$$

where $E^C = E^R + iE^I$,

$$S(\omega) = \frac{1}{1 + \dfrac{\pi i\omega\eta d}{2wE}\left(\dfrac{E}{E^C} - \nu^2\right)} \tag{38}$$

and N is the number of cracks per unit area. For the hexagonal array shown in Fig. 2, $Nd^2 = 2/\sqrt{3}$. Using $G^C = E^C/2(1+\nu^C)$ and (16), i.e. $E^C/(1-\nu^C) = E/(1-\nu)$, one finds

$$\frac{G^C}{G} = \frac{\nu + 1}{(\nu - 1) + \dfrac{2E}{E^C}}. \tag{39}$$

For $\omega = 0$, (39) gives the ratio of the completely relaxed to the unrelaxed shear modulus, $\bar{G}/G$. As we mentioned at the end of Section 3, this result is almost identical to that of Raj and Ashby, see Fig. 3.

The imaginary part of G^C/G is plotted in Fig. 6(a). It can be seen that the maximum of G^I occurs at a value of ω slightly less than that for finite element results. For comparison, a Debye peak is also fitted to the self-consistent results. This is done by using (30) and (31), where $\delta G/G = 1 - \bar{G}/G$ is given by (39) at $\omega = 0$ and ω_c is the approximate frequency at which G^I/G is a maximum.

5. A SELF-CONSISTENT THEORY FOR SPHERICAL GRAINS

The self-consistent theory has been successfully used to predict the macroscopic properties of polycrystalline aggregates from the knowledge of single crystal behavior. It has also been applied to composite materials. For a list of references see [5, 6, 15–19]. In this section we consider a self-consistent theory for grain boundary sliding. It is assumed that the grain material is linear elastic and isotropic. Our purpose is to find $\bar{G}/G$ as a function of ν when the grain boundaries slide freely.

Energetic approach

The arguments of the self-consistent theory will be given along the same lines as Eshelby [19]. Consider a large homogeneous body with elastic constants $\bar{G}$ and $\bar{\nu}$. First assume a uniform tension, $\bar{\sigma}_z = P$, as the macroscopic state of stress. Let, simultaneously, a small spherical portion of the material be replaced by a spherical inhomogeneity of exactly the same size but with the local constants G and ν. Across the interface, the shearing stress is to vanish and the normal displacement is to be continuous. We demand that there be no net change of strain energy as a result of this process. This provides one equation relating $\bar{G}$, $\bar{\nu}$ to G, ν. Next, let the overall state of stress be hydrostatic. Then, no sliding will occur in the polycrystal since the shearing stress is zero everywhere. Therefore, the relaxed elastic bulk modulus, $\bar{K}$, is the same as the unrelaxed, K

$$\bar{K} = K \quad \text{or} \quad \frac{\bar{G}(1+\bar{\nu})}{1-2\bar{\nu}} = \frac{G(1+\nu)}{1-2\nu}. \tag{40}$$

This gives the second equation relating $\bar{G}$, $\bar{\nu}$ to G, ν.

The above stated change in energy is the interaction energy of the inhomogeneity with the applied stress. In the classical approach to the self-consistent method, Eshelby's inhomogeneity problem [19] is used to calculate this interaction energy. But this is not possible in the present case since in Eshelby's problem the interface between the inhomogeneity and the matrix is

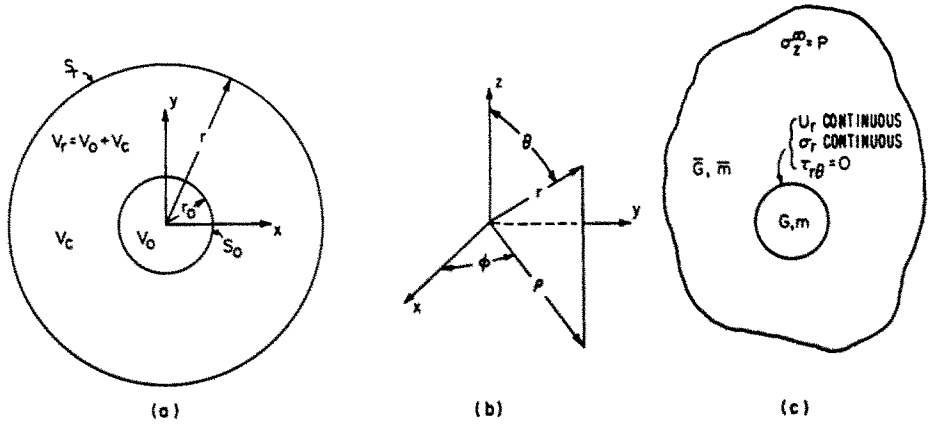

Fig. 8. (a) Definition of V_r, V_0 and V_c, (b) spherical coordinates, (c) boundary conditions.

welded (no sliding being possible) whereas here this interface is free to slide. Therefore, the following auxiliary problem must first be solved.

Let (r, θ, ϕ) denote the spherical coordinates as shown in Fig. 8(b). In region $r < r_0$, which will be referred to as the inhomogeneity or the inclusion, the elastic constants are G and ν. In $r > r_0$, which will be called the matrix, the elastic constants are $\bar{G}$ and $\bar{\nu}$. The state of stress at $r = \infty$ is uniform tension in the z-direction, $\sigma_z^\infty = P$. The boundary conditions at $r = r_0$ are that $\tau_{r\theta} = 0$ and that the normal component of the displacement and traction vectors be continuous across the boundary. Notice that because of axial symmetry $\tau_{r\phi} = 0$ everywhere.

The solution to this problem is obtained by using Papkovich–Neuber harmonic potentials. Expressing the prescribed stresses on the boundary in terms of spherical harmonics, one obtains the solution for the stresses and displacements also in terms of spherical harmonics. This solution consists of two parts: the solutions to the internal problem for the solid sphere and to the external problem for the elastic space outside the spherical inclusion. The details are given in A.4 of the Appendix.

Returning again to the self-consistent analysis, let the uniform stress at infinity be denoted by σ_{ij}^∞; then ϵ_{ij}^∞ is related to σ_{ij}^∞ by $\epsilon_{ij}^\infty = \bar{M}_{ijkl}\sigma_{ij}^\infty$, where $\bar{M}_{ijkl}$ is the compliance of the matrix. The condition that the relaxed spherical inclusion gives rise to no net change in energy is

$$\lim_{r\to\infty} \int_{V_r} (\sigma_{ij}\epsilon_{ij} - \sigma_{ij}^\infty \epsilon_{ij}^\infty)\, dV = 0 \tag{41}$$

where V_r is the region occupied by a sphere of radius r; see Fig. 8(a). We will use the auxiliary solution to explicitly evaluate eqn (41), but first it is convenient to transform this equation into a form which is more amenable to calculations.

It can be shown that eqn (41) is equivalent to

$$\epsilon_{ij}^\infty \int_{V_0} \sigma_{ij}\, dV + \sigma_{ij}^\infty \int_{S_0} U_i^{(e)} n_j\, dS - 2V_0 \sigma_{ij}^\infty \epsilon_{ij}^\infty = 0 \tag{42}$$

where V_0 and S_0 are the volume and the surface of the inclusion and the superscript (e) means external. But since $\sigma_{33}^\infty = P$ and $\sigma_{ij}^\infty = 0$ otherwise, (42) becomes

$$\frac{-P\bar{\nu}}{\bar{G}(1+\bar{\nu})} \int_{V_0} \sigma_x\, dV + \frac{P}{2\bar{G}(1+\bar{\nu})} \int_{V_0} \sigma_z\, dV + P \int_{S_0} U_3^{(e)} n_3\, dS - V_0 \frac{P^2}{\bar{G}(1+\bar{\nu})} = 0. \tag{43}$$

This equation, which can easily be evaluated in terms of ν, $\bar{\nu}$, G, and $\bar{G}$ by using the auxiliary solution, is the desired form of (41).

Evaluation of various terms in (43) involves long but straightforward calculations. By using appropriate formulas, the volume integrals must first be converted into integrals over the surface of the sphere. Then, substituting the values for stresses and displacements from the

auxiliary solution and performing the integrations, after considerable algebra one arrives at

$$\left[(1+\nu)(1-2\bar{\nu})+\frac{\bar{G}}{G}(1+\bar{\nu})(1-2\nu)\right]\frac{2GA_0}{P}+$$
$$\left[(7+5\nu)\frac{13+\bar{\nu}}{7-5\bar{\nu}}+4(7-4\nu)\frac{\bar{G}}{G}\right]\frac{Gr_0^2A_2(1+\bar{\nu})}{5P}-3(1+\bar{\nu})\cdot\frac{1-\bar{\nu}}{7-5\bar{\nu}}+1=0 \quad (44)$$

where A_0 and A_2 are constants given in (A.28) and (A.30). Equation (44) is one relation between ν, $\bar{\nu}$, G, and $\bar{G}$. The second relation is (40). Solving these two equations simultaneously and simplifying the results substantially, one obtains

$$\begin{cases}\dfrac{\bar{G}}{G}=\dfrac{7+5\nu}{4(7-4\nu)}\\[2ex] \bar{\nu}=\dfrac{4(7-4\nu)(1+\nu)-(7+5\nu)(1-2\nu)}{8(7-4\nu)(1+\nu)+(7+5\nu)(1-2\nu)}.\end{cases} \quad (45)$$

These give the final result. It is interesting to note that $\bar{G}/G$ as given by the above equations is exactly $\frac{5}{8}$ times the result obtained from Zener's eqn (1). For $\nu=\frac{1}{3}$, (45) gives $\bar{G}/G=0.38$. This value for $\bar{G}/G$ is smaller than that predicted by experiments on equiaxial polycrystals with uniform grain size[4, 13, 20]. This is caused by the absence of geometrical impediments (such as grain corners) to sliding at the boundary of a spherical grain. In the classical self-consistent theory where no sliding takes place, the assumption of spherical grains leads to plausible results; but here this assumption leads to a great overestimation of the extent of relaxation caused by grain boundary sliding. Here the properties of the surface are critical.

Stress and strain averaging

Expressions for average stress and strain inside a homogeneous body which contains N surfaces $S_\alpha(\alpha=1, N)$ along which the shearing traction vanishes have been derived in[8]. It is shown that the average stress is

$$\bar{\sigma}_{ij}=\frac{1}{V}\int_V \sigma_{ij}\,dV \quad (46)$$

where V is the volume of the body. The average strain on the other hand is given by

$$\bar{\epsilon}_{ij}=\frac{1}{V}\int_V \epsilon_{ij}\,dV+\sum_{\alpha=1}^{N}\int_{S^+}\frac{1}{2}[(U_i^+-U_i^-)n_j^+ +(U_j^+-U_j^-)n_i^+]\,dS_\alpha^+ \quad (47)$$

where S_α^+ is the side of S_α whose unit normal is $\mathbf{n}^+$. The second term, which depends on the jump in the tangential component of the displacement across $S_\alpha(\alpha=1, N)$, is the contribution to total strain due to sliding.

Now instead of using (41) as the self-consistent criterion we use the alternative postulate

$$\sigma_{ij}^{\infty}=\frac{1}{V_0}\int_{V_0}\sigma_{ij}\,dV \quad (48)$$

i.e. we require that stress at infinity be the same as the average stress in the inclusion. But $\sigma_{33}^{\infty}=P$ and $\sigma_{ij}^{\infty}=0$ otherwise. Setting the averages over the inclusion of σ_z and σ_x respectively equal to P and 0, converting the volume integrals into surface integrals, using the auxiliary solution, and carrying out the integrations, one obtains a system of two equations and two unknowns. (Notice that the averages of σ_{ij} for $i\neq j$ vanish identically.) The solution of this system is the same as (45). Thus the stress averaging approach is completely equivalent to the energetic statement of the self-consistent theory.

It can easily be established that the strain averaging approach is also equivalent to the energetic approach. In fact, by using the energy criterion (41) we arrived at (42), but by what

has been said, (42) and (48) are satisfied simultaneously. Substituting (48) into (42) and simplifying, one gets

$$\sigma_{ij}^{\infty} = \frac{1}{V_0}\int_{V_0} \epsilon_{ij}\, dV + \frac{1}{V_0}\int_{S_0} \frac{1}{2}[(U_i^{(e)} - U_i^{(i)})n_j + (U_j^{(e)} - U_j^{(i)})n_i]\, dS \tag{49}$$

where superscript (e) and (i) mean external and internal and n is the unit outward normal to the surface of the inclusion. Now, comparing (49) with (47) we see that (49) is, indeed, the expression of self-consistent criterion for strain averaging. It states that strain at infinity is equal to the average strain in the inclusion plus a term which depends on the jump in the tangential displacement across the boundary. This term is the contribution to total strain due to sliding.

Therefore, the three approaches (energy, stress, and strain) lead to one and the same result, hence justifying the designation "self-consistent". This situation is reminiscent of a similar circumstance in the classical self-consistent theory, where it was proved by Hill[15] that these various approaches are equivalent.

Connection between the Zener and the self-consistent theories

Consider the equation

$$\int_{V_r} (\sigma_{ij}\epsilon_{ij} - \bar{\sigma}_{ij}\bar{\epsilon}_{ij})\, dV = 0 \tag{50}$$

where V_r is the volume of sphere with radius r (see Fig. 8a), $\bar{\sigma}_{ij}$ is the average stress over V_r, $\bar{\epsilon}_{ij} = \bar{M}_{ijkl}\bar{\sigma}_{kl}$, $\epsilon_{ij} = M_{ijkl}\sigma_{kl}$, and $\bar{M}_{ijkl}$ and M_{ijkl} are the overall and the local compliances. Letting $r = r_0$, (50) becomes the same as Zener's method applied to the inclusion. Using the solution to the internal problem in A.4 after a lengthy but straightforward calculation, one can show that (50) (for $r = r_0$) leads exactly to Zener's result, i.e. eqn (1). (This is so in spite of the fact that the state of stress for Zener's solution[4] is different from that obtained from the solution to the internal problem.) However, as r increases it is obvious that $\bar{\sigma}_{ij}$ approaches σ_{ij}^{∞}, and (50) becomes the same as the self-consistent eqn (41). In fact, by only letting $r = 1.5\, r_0$ it was found numerically that (50) gives a solution which is to within one percent of the self-consistent result (45). Therefore, the self-consistent theory is seen to be the same as Zener's method applied to the polycrystal as a whole and not to an isolated grain. The connection between the two theories is thus established.

Acknowledgements—The author wishes to thank Professors J. W. Hutchinson and B. Budiansky for their advice and encouragement. This work was supported in part by the Air Force Office of Scientific Research under Grant AFOSR 73-2476, by the National Science Foundation under Grant ENG 76-04019, and by the Division of Applied Sciences, Harvard University.

REFERENCES

1. C. Zener, *Elasticity and Anelasticity of Metals*. The University of Chicago Press, Chicago (1948).
2. H. Gleiter and B. Chalmers, *High-Angle Grain Boundaries*. Pergamon Press, England (1972).
3. D. Mclean, *Grain Boundaries in Metals*. Oxford University Press, England (1975).
4. C. Zener, Theory of elasticity of polycrystals with viscous grain boundaries. *Phys. Rev.* 60, 906 (1941).
5. R. J. O'Connell and B. Budiansky, Viscoelastic properties of fluid-saturated cracked solids. *J. Geophys. Res.* 82, 5719 (1977).
6. B. Budiansky and R. J. O'Connell, Elastic moduli of a cracked solid. *Int. J. Solids Structures* 12, 81 (1976).
7. F. W. Crossman and M. F. Ashby, The non-uniform flow of polycrystals by grain-boundary sliding accommodated by power-law creep. *Acta Met.* 23, 425 (1975).
8. F. Ghahremani, An analysis of grain boundary sliding, Harvard University Ph.D. Thesis (1978).
9. S. G. Lekhnitskii, *Theory of Elasticity of an Anisotropic Elastic Body*, Holden-Day, San Francisco (1963).
10. R. Raj and M. F. Ashby, On grain boundary sliding and diffusional creep. *Met. Trans.* 2, 1113 (1971).
11. M. A. Biot, Theory of stress–strain relations in anisotropic viscoelasticity and relaxation phenomena. *J. Appl. Phys.* 25, 1385 (1954).
12. T. S. Kê, Experimental evidence of the viscous behavior of grain boundaries in metals. *Phys. Rev.* 71, 533 (1947).
13. A. S. Nowick and B. S. Berry, *Anelastic Relaxation in Crystalline Solids*. Academic Press, New York (1972).
14. A. D. N. Smith, *R. A. E. Report 55* (1950).
15. R. Hill, Continuum micro-mechanics of elastoplastic polycrystals. *J. Mech. Phys. Solids* 13, 89 (1965).
16. R. Hill, A self-consistent mechanics of composite materials. *J. Mech. Phys. Solids* 13, 213 (1965).

17. J. W. Hutchinson, Bounds and self-consistent estimates for creep of polycrystalline materials. *Proc. Roy. Soc. Lond. A.* **384**, 101 (1976).
18. J. W. Hutchinson, Elastic-plastic behavior of polycrystalline metals and composites. *Proc. Roy. Soc. Lond. A.* **319**, 247 (1970).
19. J. D. Eshelby, The determination of the elastic field of an ellipsoidal inclusion and related problems. *Proc. Roy. Soc. Lond. A.* **241**, 376 (1957).
20. D. T. Peters, J. C. Bisseliches and J. W. Spretnak, Some observations of grain boundary relaxation in copper and copper-2 Pct cobalt. *Trans. AIME*, **230**, 530 (1964).
21. N. I. Muskhelishvili, *Some Basic Problems of the Mathematical Theory of Elasticity*. Noordhoff (1975).
22. A. I. Lur'e, *Three-Dimensional Problems of the Theory of Elasticity*. Interscience Publishers, New York (1964).
23. C. S. Desai and J. F. Abel, *Introduction to the Finite Element Method*. Van Nostrand Reinhold, New York (1972).
24. O. C. Zienkiewicz, *The Finite Element Method*, 3rd Edn. McGraw-Hill, New York (1978).

APPENDIX

A.1 *Finite element calculations for linear analysis*

The grid used in the calculations is shown in Fig. 3(a). It consists of constant strain triangles and quadrilaterals made up of four such triangles. Figure 3(c) shows a typical quadrilateral element. Coordinates of point M are the averages of coordinates of points A, B, C and D. After finding the 10×10 stiffness matrix of this element, node M is condensed[23] and the stiffness matrix of the quadrilateral is obtained in terms of the displacements at the four corner nodes. The element stiffness matrices are then assembled according to the direct stiffness method to obtain the overall stiffness matrix $[K]$. The element and the overall stiffness matrices (which are symmetric and positive definite) and load vectors are consistent with the principle of minimum potential energy. The equilibrium equation for the assemblage is

$$[K]\{q\} = \{Q\} \tag{A.1}$$

where $\{q\}$ and $\{Q\}$ are the vector of nodal displacements and the load vector, respectively. The details of the derivation of this equation will not be given here since they can be found in numerous text-books on finite element method, e.g.[23, 24].

The boundary conditions (3) can be implemented easily by the usual methods. For example, for nodes on IP of Fig. 2(a), to apply $\tau_{xy} = 0$ we simply make the tangential component of the load vector on these nodes equal to zero. To implement $V = v$ for degree of freedom i say, $q_i = v$, we first modify the load vector according to

$$Q_j' = Q_j - K_{ji}v \quad \text{for} \quad i \neq j \quad \text{and} \quad Q_i' = v. \tag{A.2}$$

Then the i-th row and the i-th column of the stiffness matrix are made zero and the diagonal element, K_{ii}, is made unity, according to standard procedures.

From the form of the boundary conditions on PQ, shown in Fig. 2(a), it follows that nodes on this side must be arranged in pairs of points equidistant from M. With the exception of nodes at P and Q, the degrees of freedom at all other nodes on PQ must be referred to the normal and tangential directions. (These statements are true also for the finite element grids used in the next section.) The tangential boundary condition, $\sigma_t = 0$, can be imposed in the usual manner. We now explain the application of the normal boundary conditions. For definiteness we consider a typical arrangement of nodes on PQ shown in Fig. 3(d). Introduce the notation

$$\begin{cases} F_x(i), F_y(i) & \text{force in the } x \text{ and } y \text{ directions on node } i \\ F_n(i), F_t(i) & \text{force in the normal and the tangential directions on node } i \\ U(i), V(i) & \text{displacements in the } x \text{ and } y \text{ directions on node } i \\ U_n(i), U_t(i) & \text{displacements in the normal and the tangential directions on node } i \\ q_i = U(1), q_2 = V(1), Q_3 = U_n(2), q_4 = U_t(2) \ldots \\ Q_1 = F_x(1), Q_2 = F_y(1), Q_3 = F_n(2), Q_4 = F_t(2) \ldots \end{cases} \tag{A.3}$$

With this notation, in terms of the nodal displacements, (5) and (6) become

$$\begin{cases} U(1) + U(6) = u \\ U_n(2) + U_n(5) = \dfrac{\sqrt{3}}{2}u + \dfrac{1}{2}v \\ U_n(3) + U_n(4) = \dfrac{\sqrt{3}}{2}u + \dfrac{1}{2}v. \end{cases} \tag{A.4}$$

Similarly (8a) for the traction gives

$$\begin{cases} F_x(1) = F_x(6) \\ F_n(2) = F_n(5) \\ F_n(3) = F_n(4). \end{cases} \tag{A.5}$$

Equations (A.4) and (A.5) are the discretized form of the boundary conditions for the particular grid shown in Fig. 3(d).

The discretized form of the constraint (10) is

$$\sum y\text{-reactions at nodes on } IP - \sum y\text{-reactions at nodes on } OQ = 0, \tag{A.6}$$

where Σ denotes the sum. Reactions at nodes on IP and OQ (see Fig. 3d) are related to nodal displacements by eqn (A.1). Therefore using (A.1) one can write (A.6) as a constraint on the displacement vector, q, i.e.

$$\sum_{i=1}^{N} C_i q_i = 0 \tag{A.7}$$

where N is the total number of degrees of freedom. This equation together with (A.4) and (A.5) completely define the boundary value problem in discretized form.

We now explain the method for imposing the boundary conditions. Consistent with (A.5) introduce the notation

$$\begin{cases} \lambda_1 \equiv F_x(1) = F_x(6) \\ \lambda_2 \equiv F_n(2) = F_n(5) \\ \lambda_3 \equiv F_n(3) = F_n(4) \end{cases} \tag{A.8}$$

where the grid shown in Fig. 3(d) will be used to illustrate the method. By virtue of the linearity of the problem, the displacement q_i is a linear function of λ_i, i.e.

$$q_i = \sum_{k=1}^{3} a_{ik}\lambda_k + q_i^0 \qquad i = 1, N \tag{A.9}$$

where a_{ik} are the displacement influence coefficients. Therefore, in order to calculate $\{q^0\}$ we solve (A.1) when $\lambda_1 = \lambda_2 = \lambda_3 = 0$. Similarly, a_{i1}, $i = 1, N$ are calculated by solving (A.1) when $\lambda_1 = 1$ and $\lambda_2 = \lambda_3 = 0$ and so on.

This procedure requires repeated solution of (A.1) for different load vectors. This can be done by first using the Choleski's method to decompose the stiffness matrix into upper and lower triangular matrices. Then, each time the load vector is changed, it is only necessary to carry out the back and forward substitutions. The computer time required to decompose the stiffness matrix is by far more than that spent on back and forward substitutions. Therefore, this process increases the cost of computations only slightly.

After calculating the influence coefficients, a_{ij}, and vector $\{q^0\}$, eqns (A.9) are inserted into (A.4) and (A.7) to obtain a system of four equations for the determination of λ_1, λ_2, λ_3, and u. Solving this system and substituting the result in (A.9), we calculate the nodal displacements and hence complete the solution of the problem. In the above discussions, for definiteness we considered the grid shown in Fig. 3(d). For a finer grid the method is exactly the same.

A.2 *Details of the finite element technique for viscoelastic analysis*

The grid is the same as before; see Fig. 3(a). Since the material inside the grains is elastic, the stiffness matrix remains real and is the same as before. The load vector, on the other hand is complex, resulting in a complex displacement vector as well. The equilibrium equation, now, is

$$[K]\{q^C\} = \{Q^C\} \tag{A.10}$$

where $\{q^C\} = \{q^R\} + i\{q^I\}$ and $\{Q^C\} = \{Q^R\} + i\{Q^I\}$ are the complex displacement and load vectors.

For definiteness we explain the boundary conditions by considering the simple grid shown in Fig. 3(d). On OQ, OI, and OP the boundary conditions can be applied easily by ordinary methods; see eqn (A.2). On PQ using (A.3), in the normal direction one finds

$$\begin{aligned} U^C(1) + U^C(6) &= u^C \\ U_n^C + U_n^C(5) &= \frac{\sqrt{3}}{2}u^C + \frac{1}{2}v^C \\ U_n^C(3) + U_n^C(4) &= \frac{\sqrt{3}}{2}u^C + \frac{1}{2}v^C \end{aligned} \tag{A.11}$$

and

$$\begin{cases} F_x^C(1) = F_x^C(6) \\ F_n^C(2) = F_n^C(5) \\ F_n^C(3) = F_n^C(4) \end{cases} \tag{A.12}$$

where (5), (6) and (8a) are used.

To discretize the tangential boundary condition (23), we first recall an elementary result. Assuming that the shearing stress σ_t varies linearly between two successive nodes i and j on the boundary, the contribution to the tangential nodal forces due to the traction on the segment ij is[23]

$$\begin{cases} F_t(i) = l\left(\dfrac{\sigma_t(i)}{3} + \dfrac{\sigma_t(j)}{6}\right) \\ \\ F_t(j) = l\left(\dfrac{\sigma_t(i)}{6} + \dfrac{\sigma_t(j)}{3}\right) \end{cases} \tag{A.13}$$

where $\sigma_t(i)$ and $\sigma_t(j)$ are the values of σ_t at nodes i and j; and l is the length of the segment ij. Referring back to the particular grid in Fig. 3(d), it can be seen that at nodes (1) and (6) $\sigma_t^C = 0$, since at these nodes the discontinuity in the tangential displacement across the boundary vanishes. Using (A.13), (A.23), and (24), one obtains the discretized form of

the tangential boundary condition on PQ as

$$\begin{cases} F_t^C(2) = i\omega \dfrac{\eta}{w}\left\{\left(\dfrac{l_1}{3}+\dfrac{l_2}{3}\right)\left[\dfrac{-1}{2}u^C + \dfrac{\sqrt{3}}{2}v^C - U_t^C(2) - U_t^C(5)\right] \right. \\ \qquad \left. + \dfrac{l_2}{6}\left[\dfrac{-1}{2}u^C + \dfrac{\sqrt{3}}{2}v^C - U_t^C(3) - U_t^C(4)\right]\right\} \\ F_t^C(3) = i\omega \dfrac{\eta}{w}\left\{\dfrac{l_2}{6}\left[\dfrac{-1}{2}u^C + \dfrac{\sqrt{3}}{2}v^C - U_t^C(2) - U_t^C(5)\right] \right. \\ \qquad \left. + \left(\dfrac{l_2}{3}+\dfrac{l_3}{2}\right)\left[\dfrac{-1}{2}u^C + \dfrac{\sqrt{3}}{2}v^C - U_t^C(3) - U_t^C(4)\right]\right\} \end{cases} \tag{A.14}$$

and

$$\begin{cases} F_t^C(5) = F_t^C(2) \\ F_t^C(4) = F_t^C(3) \end{cases} \tag{A.15}$$

where l_1, l_2, l_3 are, respectively, the distances between the nodes 1 and 2, 2 and 3, 3 and 4 on the boundary PQ.

The constraint (10) leads to

$$\sum_{i=1}^{N} C_i q_i^C = 0. \tag{A.16}$$

Derivation of this parallels that of (A.7). The coefficients C_i in (A.16) are exactly the same as in (A.7). The finite element version of the boundary value problem is now completely defined.

To incorporate the boundary conditions on PQ, the method used in the previous section will be utilized. Let $\lambda_i^C (i = 1, 5)$ be defined as

$$\begin{cases} \lambda_1^C = F_x^C(1) = F_x^C(6) \\ \lambda_2^C = F_n^C(2) = F_n^C(5) \\ \lambda_3^C = F_n^C(3) = F_n^C(4) \\ \lambda_4^C = F_t^C(2) = F_t^C(5) \\ \lambda_5^C = F_t^C(3) = F_t^C(4). \end{cases} \tag{A.17}$$

The displacements q_i^C are then given by

$$q_i^C = \sum_{k=1}^{5} a_{ik}\lambda_k^C + q_i^0. \tag{A.18}$$

The coefficients a_{ij} and the vector $\{q^0\}$ turn out to be real. To calculate them, exactly the same method as before can be used. That is, we first set $\lambda_i = 0$ $(i = 1, 5)$ and solve (A.10) to calculate $\{q^0\}$. Next we set $\lambda_1 = 1$ and $\lambda_i = 0$ otherwise to find a_{ij} $(i = 1, N)$ and so on. Substituting (A.18) into (A.11), (A.14), and (A.16), a system consisting of six complex equations is obtained for the determination of λ_i^C $(i = 1, 5)$ and u^C. After solving this system, from (A.18) the nodal displacements are known and the problem is solved. If ω is changed, only the boundary condition (A.14) is affected; all other equations, including (A.18) remain the same. Therefore to find the response of the material, one only has to repeatedly solve the above 6 by 6 complex system for different values of ω. The above discussions were made in reference to the simple mesh shown in Fig. 3(d). For the grid actually used in calculations (Fig. 3a) the method is exactly the same.

A.3 *Zener's calculations in two dimensions*

Assuming that the grains are circles in plane strain rather than spheres, Zener's calculations will be carried out. Consider the region inside the circle with radius r_0. The center of the circle coincides with the origin of the xy-plane, and the material inside it is linear and isotropically elastic.

Corresponding to the three solutions of Zener[4], we superimpose three solutions: (I) a uniform stress $\sigma_y = P$ and all other components of the stress vanishing, (II) a solution so chosen as to neutralize the shearing stress due to solution (I) at $r = r_0$ and (III) a solution so chosen as to neutralize the average of σ_x introduced by (II). In order that no new shearing stresses be introduced at $r = r_0$, the third solution must be isotropic in the xy-plane (i.e. $\sigma_x^{III} = \sigma_y^{III}$ and $\tau_{xy}^{III} = 0$).

We solve this problem by superposition using Muskhelishvili's complex potentials. The solution is

$$\begin{cases} \phi_I(Z) = \dfrac{P}{4}Z; \quad \phi_{II}(Z) = \dfrac{-P}{12}\dfrac{Z^3}{r_0^2}; \quad \phi_{III}(Z) = \dfrac{-P}{8}Z \\ \psi_I(Z) = \dfrac{P}{2}Z; \ \psi_{II}(Z) = 0; \qquad \psi_{III}(Z) = 0 \end{cases} \tag{A.19}$$

where the ϕ's and the ψ's are regular functions of the complex variable $Z = x + iy$, and $i = \sqrt{-1}$. Using standard formulas from[21] to calculate the stresses produced by (A.19), one may easily verify that (A.19) gives the solution. The complete solution, $\phi = \phi_I + \phi_{II} + \phi_{III}$ and $\psi = \psi_I + \psi_{II} + \psi_{III}$ is

$$\begin{aligned} \phi(Z) &= \frac{P}{8}Z - \frac{P}{12}\frac{Z^3}{r_0^2} \\ \psi(Z) &= \frac{P}{2}Z. \end{aligned} \tag{A.20}$$

The average elastic energy per grain is

$$\bar{W} = \frac{1}{A}\int_A \frac{1}{2}\sigma_{\alpha\beta}\epsilon_{\alpha\beta}\,dA = \frac{1}{2A}\int_\Gamma \sigma_r U_r\,dS \qquad (\alpha,\beta = 1,2) \tag{A.21}$$

where A is the area of the circle and Γ its contour. Using the solution (A.20) and carrying out the integrations, one finds

$$\bar{W} = \frac{P^2}{48}\cdot\frac{(9-10\nu)(1+\nu)}{E}. \tag{A.22}$$

On the other hand, the macroscopic strain energy per unit area is $\bar{W} = \bar{\sigma}_y\bar{\epsilon}_y/2$, where $\bar{\sigma}_y$ is the average of σ_y over A and

$$\bar{\epsilon}_y = \left(\frac{1}{\bar{E}} - \frac{\nu^2}{E}\right)\bar{\sigma}_y.$$

This last relation is obtained from (15) by noting that the overall response is transversely isotropic as we have explained before (see comments following eqn 15). Using the solution (A.20), one gets

$$\bar{\sigma}_y = \frac{1}{A}\int_A \sigma_y\,dA = \frac{r_0}{A}\int_\Gamma \sigma_r n_y^2\,dS = \frac{P}{2} \tag{A.23}$$

and therefore

$$\bar{W} = \frac{P^2}{8}\left(\frac{1}{\bar{E}} - \frac{\nu^2}{E}\right). \tag{A.24}$$

Setting the microscopic and the macroscopic expression for $\bar{W}$ (eqns A.22 and A.24) equal to each other and solving for $\bar{E}/E$, one gets

$$\frac{\bar{E}}{E} = \frac{6}{9-\nu-4\nu^2}. \tag{A.25}$$

Using (16) and (A.25) together with $G = E/2(1+\nu)$, one obtains the final result

$$\frac{\bar{G}}{G} = \frac{3}{2(3-2\nu)}. \tag{A.26}$$

This expression is plotted as the curve labelled (3) in Fig. 4.

A.4 *Solution of the auxiliary problem*

An isotropic elastic medium, containing a spherical region (the inclusion) with different elastic constants than those of the remainder, is subjected to uniform tension at infinity. Across the interface the shearing stress vanishes and the normal displacement is continuous; see Fig. 8(c). The objective is to find the state of stress, the displacements, etc. everywhere.

The two-dimensional version of this problem is solved in the book by Muskhelishvili[21], Article 58. The three-dimensional problem will be solved by superposition making use of a general form for the solution of the problem of the equilibrium of a symmetrically loaded elastic sphere, constructed in the book by Lur'e[22], *Three-Dimensional Problems of the Theory of Elasticity*, Chapter 6.

Let the elastic constants of the matrix be $\bar{G}$ and $\bar{\nu}$ and those of the inclusion G and ν. Let the radius of the sphere be r_0 and its center coincide with the origin. First the problem of a spherical cavity in an infinite medium with uniform tension at infinity will be solved. It will be noticed that at $r = r_0$ (i.e. on the surface of the cavity) the normal displacement U_r due to this solution is of the form $U_r = a_0P_0(\mu) + a_2P_2(\mu)$, where a_0 and a_2 are constants and $P_0(\mu) = 1$, $P_2(\mu) = (3\mu^2 - 1)/2$ are the Legendre polynomials of order zero and two and $\mu = \cos\theta$. For $n = 0, 1, 2, \ldots$ the above mentioned general representation has the property that an applied stress $\sigma_r = \sigma_nP_n(\mu)$ on the boundary (of the cavity or of the solid sphere) leads to displacements U_r proportional to $P_n(\mu)$, and solutions for different n are completely uncoupled from each other. We apply a stress $\sigma_r = \sigma_0P_0(\mu) + \sigma_2P_2(\mu)$ at $r = r_0$ both to the interior of the cavity and to the surface of the solid sphere; σ_0 and σ_2 will then be so chosen as to make U_r continuous at $r = r_0$. At this stage at $r = r_0$, $\tau_{r\theta} = 0$, and U_r and σ_r are continuous. Every condition is therefore satisfied, and the problem is completely solved. We give the final results; for more details see[8].

Internal problem

The solution to the internal problem is composed of two parts. The first part is

$$\begin{cases} U_r = -2A_0(1-2\nu)r, \quad U_\theta = 0 \\ \sigma_r = \sigma_\theta = \sigma_\phi = -4GA_0(1+\nu), \quad \tau_{r\theta} = 0 \end{cases} \tag{A.27}$$

where

$$A_0 = \frac{-P(1-\bar{\nu})}{4(1+\bar{\nu})[(2\bar{G}+G) + \nu(G-4\bar{G})]}. \tag{A.28}$$

The second part is

$$\begin{cases} U_r = [12A_2 r^3 \nu + 2B_2 r]P_2(\mu) \\ U_\theta = [A_2 r^3(7-4\nu) + B_2 r]\dfrac{dP_2}{d\theta} \\ \dfrac{1}{2\bar{G}}\sigma_r = [-6A_2 r^2 \nu + 2B_2]P_2(\mu) \\ \dfrac{1}{2\bar{G}}\tau_{r\theta} = [A_2 r^2(7+2\nu) + B_2]\dfrac{dP_2}{d\theta} \end{cases} \tag{A.29}$$

where

$$\begin{cases} A_2 = \dfrac{10P(1-\bar{\nu})}{r_0^2[4\bar{G}(7-5\bar{\nu})(4\nu-7) - G(17-19\bar{\nu})(7+5\nu)]} \\ B_2 = -(7+2\nu)r_0^2 A_2. \end{cases} \tag{A.30}$$

Similar but somewhat more involved expressions hold for σ_ϕ and σ_θ which we shall not write since they will not be used.

External problem

The solution to the external problem consists of three parts. The first part is due to the uniform state of stress $\sigma_Z^\infty = P$

$$\mathbf{U}^\infty = \frac{-P}{2\bar{G}(1+\bar{\nu})}(\bar{\nu}x\mathbf{i} + \bar{\nu}y\mathbf{j} - z\mathbf{k}) \tag{A.31}$$

where i, j and k are unit vectors in the x, y, and z-directions. The r-component of (A.31) is

$$U_r^\infty = \frac{Pr_0}{6\bar{G}}\left[\frac{1-2\bar{\nu}}{1+\bar{\nu}}P_0(\mu) + 2P_2(\mu)\right] \quad (\mu = \cos\theta). \tag{A.32}$$

The components of the stress tensor are

$$\begin{cases} \sigma_r^\infty = P\cos^2\theta, \qquad \sigma_\theta^\infty = P\sin^2\theta \\ \tau_{r\theta}^\infty = -P\sin\theta\cos\theta, \sigma_\phi^\infty = 0. \end{cases} \tag{A.33}$$

The second part is

$$\begin{cases} U_r = -\dfrac{\tilde{D}_0}{r^2}, \quad U_\theta = 0, \quad \sigma_r = \dfrac{4\bar{G}\tilde{D}_0}{r^3} \\ \sigma_\theta = \sigma_\phi = -\dfrac{2\bar{G}\tilde{D}_0}{r^3}, \quad \tau_{r\theta} = 0 \end{cases} \tag{A.34}$$

where $\tilde{D}_0 = D_0' + D_0$, $D_0' = -Pr_0^3/12\bar{G}$, $D_0 = -A_0 r_0^3(1+\nu)G/\bar{G}$ and A_0 is given in (A.28).

The third part is

$$\begin{cases} U_r = \left[\dfrac{2\tilde{C}_2(5-4\bar{\nu})}{r^2} - \dfrac{3\tilde{D}_2}{r^4}\right]P_2(\mu) \\ U_\theta = \left[\dfrac{2\tilde{C}_2(1-2\bar{\nu})}{r^2} + \dfrac{\tilde{D}_2}{r^4}\right]\dfrac{dP_2}{d\theta} \\ \dfrac{1}{2\bar{G}}\sigma_r = \left[-\dfrac{4\tilde{C}_2(5-\bar{\nu})}{r^3} + \dfrac{12\tilde{D}_2}{r^5}\right]P_2(\mu) \\ \dfrac{1}{2\bar{G}}\tau_{r\theta} = \left[\dfrac{2\tilde{C}_2(1+\bar{\nu})}{r^3} - \dfrac{4\tilde{D}_2}{r^5}\right]\dfrac{dP_2}{d\theta} \end{cases} \tag{A.35}$$

where $\tilde{C}_2 = C_2' + C_2$, $\tilde{D}_2 = D_2' + D_2$,

$$\begin{cases} C_2' = \dfrac{5P}{12\bar{G}} \cdot \dfrac{r_0^3}{7-5\bar{\nu}}; \quad D_2' = \dfrac{P}{2\bar{G}} \cdot \dfrac{r_0^5}{7-5\bar{\nu}} \\ C_2 = \dfrac{G}{\bar{G}} \cdot \dfrac{7+5\nu}{7-5\bar{\nu}} r_0^3 A_2; \quad D_2 = \dfrac{G}{2\bar{G}} - \dfrac{1+\bar{\nu}}{7-5\bar{\nu}}(7+5\nu)r_0^2 A_2. \end{cases} \tag{A.36}$$

Expressions for σ_θ and σ_ϕ are not written.

This completes the solution of the auxiliary problem. In contrast to Eshelby's problem[19], for which the state of stress in the inclusion is uniform, in the present case the stresses are composed of a uniform part and a part which varies with r like r^2.